

## LETTER TO THE EDITOR

# The nearest neutral gas phase to Supermassive Black Holes

## A massive (neutral-atom/molecule)-rich Broad Line Region in AGNs

Thi W.-F.<sup>1</sup> and Papadopoulos, P. P.<sup>2,3,4</sup><sup>1</sup> Max Planck Institute for Extraterrestrial Physics, Giessenbachstrasse, 85741 Garching, Germany e-mail: wingfai.thi@googlemail.com<sup>2</sup> Department of Physics, Section of Astrophysics, Astronomy and Mechanics, Aristotle University of Thessaloniki, GR-54124 Thessaloniki, Greece e-mail: padelis@auth.gr<sup>3</sup> Research Center for Astronomy, Academy of Athens, Soranou Efesiou 4, GR-11527 Athens, Greece<sup>4</sup> School of Physics and Astronomy, Cardiff University, Queens Buildings, The Parade, Cardiff CF24 3AA, UK

... ; ....

## ABSTRACT

**Context.** The Broad Line Regions (BLRs) are regions containing gravitationally bound gas within  $r \sim (\text{few}) \times (10^2 - 10^3)R_S$  (Schwarzschild radii) near Supermassive Black Holes (SMBHs) in Active Galactic Nuclei (AGNs). Photo-ionized by strong non-stellar AGN continuum, this gas emits luminous UV/optical/near-IR lines from ionized Hydrogen (and other multi-ionized atoms) that have the widest velocity profiles observed in galaxies, uniquely indicating the deep gravitational wells of SMBHs.

**Aims.** Nearly all BLR studies focus on its ionized gas phase (hereafter BLR<sup>+</sup>), with typical masses of only  $\sim (\text{few}) \times (10 - 100) M_\odot$ , despite strong indications of neutral BLR gas reservoirs (hereafter BLR<sup>0</sup>) with  $M_{\text{BLR}^0} \sim 10^{5-6} M_\odot$ .

**Methods.** The photoionization code CLOUDY, with its chemistry augmented with three-body reactions, is used to explore 1-D models of dustless BLRs, focusing on the BLR<sup>0</sup> conditions, and the abundances of its most prevalent neutral atoms and molecules.

**Results.** A (neutral-atom/molecule)-rich BLR<sup>0</sup> gas phase is found underlying the BLR<sup>+</sup>, the latter occupying only a thin outer layer of AGN-irradiated gas column densities, while the former contains the bulk of the BLR gas mass. Atomic carbon and oxygen and the CO molecule can reach substantial abundances in the BLR<sup>0</sup>, while their lines at IR/submm wavelengths can yield new probes of the BLR physical conditions and dynamics, unhindered by the dust absorption from outer AGN tori that readily absorbs the BLR<sup>+</sup> optical/far-UV lines.

**Conclusions.** (Neutral-atom)-rich and even molecule-rich gas can exist in the BLR<sup>0</sup>. The corresponding spectral lines from neutral atoms and molecules promise a new spectral window of gas dynamics in the vicinity of SMBHs unhindered by dust absorption, and may even allow novel tests of General Relativity in strongly curved spacetimes.

**Key words.** galaxies: active – quasars: emission lines – ISM: molecules – ISM: atoms – quasars: general – AGN: BLR

## 1. Introduction

The probability of a neutral-atomic or even molecule-rich gas phase with any significant mass lying in the vicinity ( $\sim (\text{few} \times 10^2 - 10^3)R_S$ ,  $R_S = 2GM_{\text{SMBH}}/c^2$ ) of Super Massive Black Holes (SMBHs) in Active Galactic Nuclei (AGN) could be naively thought as being virtually zero given the extreme UV and hard X-ray non-stellar continua emanating from the SMBH accretion disks and their hot coronae, e.g. Rokaki, Boisson, & Collin-Souffrin (1992); Thomas et al. (2016); Dewangan et al. (2021). The strong UV AGN continuum photoionizes such gas, sublimating its concomitant dust once its temperature rises above the sublimation limit  $T_{\text{dust}} \sim (1500 - 2000) \text{ K}$ , reached for distances of  $r \leq R_{\text{sub}} \sim 0.2[L_{\text{bol}}/(10^{46} \text{ erg s}^{-1})]^{1/2} \text{ pc}$  from the AGN (e.g., Baskin & Laor 2018). Photoionized gas seems an unlikely phase for the onset of a (neutral-atom/molecule)-rich chemistry, and even a neutral but dustless gas phase would also seem so, given the role of dust in catalysing H<sub>2</sub> formation (Gould & Salpeter 1963; Cazaux & Tielens 2002; Thi et al. 2020, and references therein).

Three important elements are missing from this simple picture, namely: a) a molecule-rich chemistry is possible even in hot dustless gas provided densities are high enough

( $n_{\text{H}} \geq 10^{10} \text{ cm}^{-3}$ ), b) molecules like H<sub>2</sub> or CO can strongly self-shield once formed even in initially small quantities and c) the thermal (and thus chemical) gas properties are drastically altered once neutral atomic and/or molecular species form, even in initially low abundances because they are efficient gas coolants via their lines. Such a molecule-rich chemistry in hot, strongly UV-irradiated dense gas, whose concomitant dust reservoir has been fully sublimated, has already been inferred in the disk around the B star 51 Oph (Thi et al. 2005, 2013), and confirmed by spatially resolved near-IR interferometric observations of CO overtone lines (Tatulli et al. 2008; GRAVITY Collaboration 2021a). CO has even been detected in the (X-ray)-irradiated gas ejecta of SN 1987A Spyromilio et al. (1988), its formation mediated by He<sup>+</sup> charge-transfer reactions (Lepp, Dalgarno, & McCray 1990) in an environment that must surely rank as among the most hostile ones in the Universe for a molecule-rich chemistry.

The possibility of a (neutral-atom/molecule)-rich gas phase in the vicinity of SMBHs, despite photo-ionization by a strong UV/X-ray AGN continuum, has been investigated earlier (Lepp et al. (1985)), but without including the very important process

of dust sublimation by the AGN radiation fields. This work was revisited by Kallman, Lepp, & Giovannoni (1987), which did not include  $\text{H}^-$  electron photo-detachment by IR radiation, another process fundamentally important for the chemistry in the strongly AGN-irradiated BLR gas. Ferland & Persson (1989), while modeling  $\text{Ca II}$  line triplet AGN observations, corrected the two aforementioned omissions, and argued for a massive neutral BLR gas phase underlying the photo-ionized one. However they did not consider any neutral-atomic or molecular abundances past the  $\text{BLR}^+/\text{BLR}^0$  boundary<sup>1</sup>, and reported  $N(\text{H})_{\min,0} \sim 10^{24.5} \text{ cm}^{-2}$  as the minimum column density necessary for explaining the  $\text{Ca II}$  triplet IR-line strengths relative to its UV lines and other lines emanating from the  $\text{BLR}^+$ . Nevertheless, the very same arguments presented by Ferland & Persson (1989), the obvious expectation that neutral-atoms/molecules will form at the deeper end of any 1-side irradiated BLR gas column densities, e.g. Gaskell (2009), as well as general arguments made throughout the AGN literature about an underlying  $\text{BLR}^0$  being much more massive than the  $\text{BLR}^+$ , e.g. Baldwin et al. (2003); Ferland (2004), all necessitate that any new state of the art BLR models extend well past the aforementioned minimum gas column density.

In this work we examine the thermal state and the abundances of a few key atomic and molecular species in a dustless  $\text{BLR}^0$ , for gas columns up to  $\sim(\text{few}) \times 10^{26} \text{ cm}^{-2}$ , and a typical AGN SED and radiation field strength. We then briefly comment on the possible use of neutral-atom and/or molecular line emission at IR/submm wavelengths as extinction-free probes of the bulk of the BLR mass, the gas velocity fields near SMBHs, and even for novel tests of General Relativity near SMBHs as recently proposed by Kostaros, Papadopoulos, & Pappas (2024).

## 2. The CLOUDY code

We utilized the CLOUDY 23.01 (Gunasekera et al. 2023) photoionisation and photodissociation code with the standard AGN input Spectral Energy Distribution (SED). CLOUDY includes photodissociation region (PDR) physics and has been benchmarked against other (PDR) codes (Röllig et al. 2007). We adopted a one-sided illuminated plan-parallel geometry. The chemical network is based on the UMIST 2012 Database for Astrochemistry with enhanced metal abundance ( $Z/Z_{\odot} = 5$ ) and specific extensions of the chemical rates (Shaw et al. 2022), specially for chemical reaction rates at  $T_{\text{gas}} \geq 100 \text{ K}$  (Shaw et al. 2023). Reactions relevant to PDR modelling are present in the CLOUDY network, including reactions with excited  $\text{H}_2$ . The default network has been complemented by relevant three-body and Calcium reactions (see Appendices A and C). The relative abundances follow the default ISM values. No grains nor PAHs are present because their temperature would be higher than their sublimation temperature in most part of the BLR, although the gas and dust temperature can be below the dust sublimation limit at very high column densities. The potential effects of any remaining dust grains in the BLR will be further explored in a forthcoming paper. In the absence of dust grains,  $\text{H}_2$ , C, and CO can only self-shield and self each other against photodissociation (Hollenbach & Tielens 1999). The cosmic-ray flux density was set to the default value.

<sup>1</sup> They made a comment only about  $\text{H}_2$  (in their Appendix), which unlike Kallman, Lepp, & Giovannoni (1987), found it to be only a trace species, but otherwise giving no abundance estimates or profiles.

## 3. The $\text{BLR}^0$ vs the $\text{BLR}^+$ : the model parameters

Ever since their discovery (Seyfert 1943), the luminous and very broad ( $FWZI \sim (10^3 - 10^4) \text{ km s}^{-1}$ ) lines of the  $\text{BLR}^+$  at UV/optical/near-IR wavelengths have been AGN signposts, revealing the deep gravitational potential of SMBHs within  $\sim(500-10^4) R_S$ . Powered by photoionization from a strong non-stellar AGN continuum that yields ionized hydrogen (and other multiply ionized atoms), these lines are used to study the BLR conditions (e.g. density, ionization, temperature and metallicity (Netzer 1990; Korista & Goad 2004; Peterson 2006; Gaskell 2009). However the sharpness of the  $\text{H}^+/\text{H}$  transition zone with,

$$\frac{\Delta R}{R_+} \sim 3.5 \times 10^{-4} \left[ \left( \frac{S_{\text{ion}}}{10^{49} \text{ s}^{-1}} \right) \left( \frac{n}{100 \text{ cm}^{-3}} \right) \right]^{-1/3}, \quad (1)$$

giving the width  $\Delta R$  of this zone (assuming a Strömgren sphere of photoionized gas of radius  $R_+$ , with  $S_{\text{ion}}$  the ionizing source's photoionization rate), *renders the  $\text{BLR}^+$  main lines, i.e. the H recombination lines, incapable of probing the  $\text{BLR}^0$ , and thus the total ( $\text{BLR}^0+\text{BLR}^+$ ) gas mass*. For e.g.  $n_{\text{H}} = 10^{11} \text{ cm}^{-3}$ :  $\Delta R/R_+ \sim 7.5 \times 10^{-7} [S_{\text{ion}}/(10^{49} \text{ s}^{-1})]^{-1/3} \ll 1$  for typical  $S_{\text{ion}}$  rates for AGN. Lines from ionized and neutral atoms with ionization potentials lower than that of H (e.g.  $\text{Fe}^+$ ,  $\text{Ca}^+$ , C, O) can probe the neutral gas past the  $\text{H}^+/\text{H}$  transition zone, yet deeper inside some can be locked into molecules, even in the absence of dust.

This leaves two questions open: a) what is the actual  $\text{BLR}^0$  gas mass, and b) what lines can probe it in its entirety. We must first adopt plausible masses for the  $\text{BLR}^0$  in order to set an  $N(\text{H})_{\max}$  value in our 1-D CLOUDY models. This is a critical parameter since, for any given AGN radiation field and SED incident on a 1-side irradiated BLR gas layer, arbitrarily large  $\text{BLR}^0$  columns can be obtained beyond the  $\text{H}^+/\text{H}$  transition zone, for a large enough  $N(\text{H})_{\max}$ . Direct  $\text{BLR}^+$  gas mass estimates via Hydrogen recombination lines give  $M_{\text{BLR}^+} \sim (10-100) M_{\odot}$ , while a set of necessarily more indirect arguments set the putative  $\text{BLR}^0$  to be at least  $M_{\text{BLR}^0} \sim (10^4-10^5) M_{\odot}$  (Baldwin et al. 2003; Gaskell 2009; Ferland 2004). On the other hand an  $N(\text{H})_{\min}$  value for BLR gas structures can be obtained by simply demanding the SMBH gravity dominates over the radiative pressure from the AGN radiation field (i.e. the BLR is gravitationally bound to the SMBH). This yields:

$$\langle N(\text{H}) \rangle > \frac{L_{\text{AGN}}}{4\pi G m_p c M_{\text{SMBH}}}, \quad (2)$$

i.e.  $N(\text{H})_{\min} \sim (10^{23}-10^{24}) \text{ cm}^{-2}$ , for typical SMBH masses  $M_{\text{SMBH}}$  and AGN luminosities  $L_{\text{AGN}}$ . Furthermore in order for the so-called radiation-pressure-confined (RPC) ionization layers to be established within the  $\text{BLR}^+$ s in a universal fashion, in pressure equilibrium with deeper neutral BLR gas layers, and do this across 8 orders of magnitude of AGN power (Baskin, Laor, & Stern 2014; Baskin & Laor 2018), it must be  $N(\text{H}) \geq 10^{24} \text{ cm}^{-2}$  (Baskin, Laor, & Stern 2014). This is similar to the  $N(\text{H})_{\min} \sim 10^{24.5} \text{ cm}^{-2}$  value deduced from the  $\text{Ca II}$  triplet line observations which trace low-ionization/neutral BLR gas layers (Ferland & Persson 1989). A maximum value for the total  $N(\text{BLR}^++\text{BLR}^0)$  column density of the various BLR gas structures can then be set simply as:  $N(\text{H})_{\max} = N(\text{H})_{\text{BLR}^+} (1 + M_{\text{BLR}^0}/M_{\text{BLR}^+}) \sim N(\text{H})_{\min} \times (10^2 - 10^4)$ . For a  $N(\text{H})_{\min} = 10^{23} \text{ cm}^{-2}$ , we adopted  $\log_{10} N(\text{H})_{\max} = 10^{26.5} \text{ cm}^{-2}$ , with a  $\log \Delta N(\text{H}) = 0.5$  grid step<sup>2</sup>, and a BLR density range of

<sup>2</sup> The exact computed column density is set by the code.

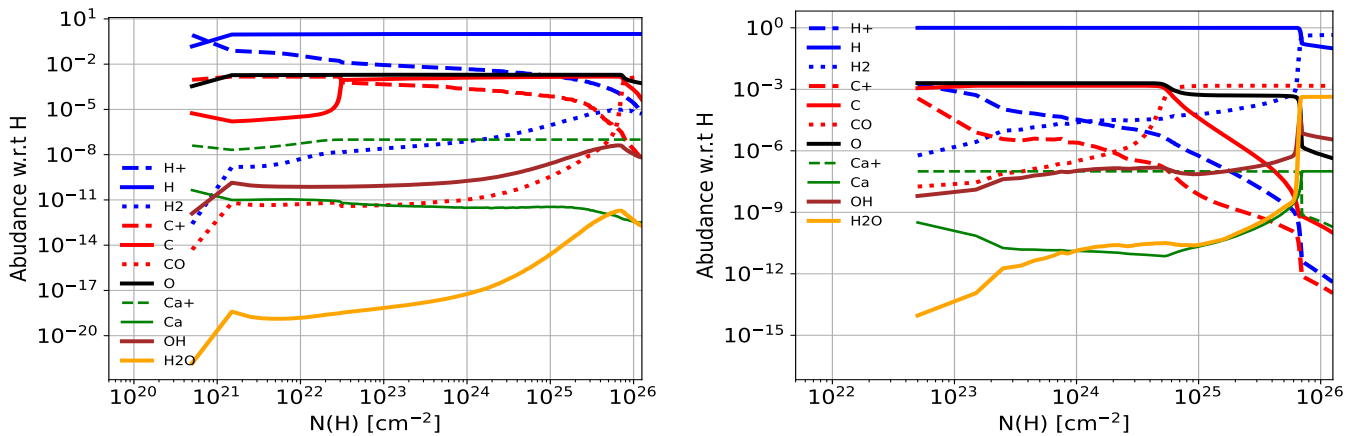


**Fig. 1.** Abundance for various species as function of the column density, *Left*: A model with  $n_{\text{H}} = 10^{12} \text{ cm}^{-3}$ ,  $\log(U) = -3$ ,  $\Delta V = 250 \text{ km s}^{-1}$ , *Right*: A model with  $n_{\text{H}} = 10^{14} \text{ cm}^{-3}$ ,  $\log(U) = -5$ ,  $\Delta V = 250 \text{ km s}^{-1}$ .

$n_{\text{H}} = (10^{10}, 10^{11}, 10^{12}, 10^{13}, 10^{14}) \text{ cm}^{-3}$ . For the ionization parameter  $U$  we adopt  $U = 0.1$  for  $n_{\text{H}} = 10^{10} \text{ cm}^{-3}$ . The other  $U$ -grid values are chosen so that the ionizing photon density  $n_{\gamma} = n_{\text{H}}U$  remains invariant, as demanded by an AGN-induced dust sublimation condition holding within BLRs in all AGN (Baskin, Laor, & Stern (2014)). We consider metallicities of  $Z/Z_{\odot}=5$ , a super-solar value being typical for BLR gas in galactic centers. Finally we adopt a typical turbulent linewidth of  $\Delta V=250 \text{ km s}^{-1}$  for the BLR gas (Gaskell 2009)<sup>3</sup>. Fine physical grids were chosen to improve the model convergence. The temperature iteration tolerance was set to  $5 \times 10^{-3}$  (the default value), while the grid parameters were: hydrogen density  $n_{\text{H}}$ , ionisation parameter  $U$ , and the total hydrogen column density  $N_{\text{H}}$ .

#### 4. Results and discussion

Figure 1 shows the abundance of various species as function of  $N(\text{H})$  for the  $n_{\text{H}} = 10^{12} \text{ cm}^{-3}$ ,  $\log(U) = -3$  model on the left panel and for the  $n_{\text{H}} = 10^{14} \text{ cm}^{-3}$ ,  $\log(U) = -5$  model on the right panel. From this figure is apparent that O and C are the two neutral atoms with the largest abundances dominating throughout the BLR<sup>0</sup> column, while deeper inside they react to form the dominant molecule expected in BLR<sup>0</sup>'s, namely CO. The latter can reach up to a relative abundance  $X(\text{CO}) \sim 10^{-4} - 10^{-3}$  deep inside BLR<sup>0</sup>'s while H<sub>2</sub> remains only a trace element as it has already been established for dust-free BLRs by Ferland & Persson (1989) and Crosas & Weisheit (1993). This is quite unlike the ordinary ISM, and indeed a (CO-rich)-yet-(H<sub>2</sub>-poor) gas phase is one of the peculiar hallmarks of a dust-free but hot and very dense gas chemistry. Evidence for exactly such chemistry has already been uncovered for the hot, dust-free, inner gas disk around the B star 51 Oph Thi et al. (2005), with CO overtone lines even used to resolve the disk at sub-au scales GRAVITY Collaboration (2021a).

From Fig. 1 we see that, for  $n_{\text{H}} = 10^{12} \text{ cm}^{-3}$ , the  $\text{H}^+ \rightarrow \text{H}$  phase transition occurs at  $N(\text{H}) \sim 10^{21} \text{ cm}^{-2}$ , with neutral atomic H remaining dominant throughout the remaining BLR<sup>0</sup> column. Only at the highest gas densities ( $n_{\text{H}} = 10^{14} \text{ cm}^{-3}$ ), and largest BLR<sup>0</sup> columns ( $N(\text{H}) \sim 5 \times 10^{25} \text{ cm}^{-2}$ ), does the neutral atomic H becomes molecular (Fig. 1). Atomic Oxygen, with its Ionization Potential (IP) of 13.618 eV only slightly above that of H

(IP=13.598 eV), can remain neutral nearly throughout the H-rich BLR<sup>0</sup> column. Atomic Carbon on the other hand, with an IP of  $\sim 11.26$  eV, can remain (singly) ionized inside the BLR<sup>0</sup> past the  $\text{H}^+ \rightarrow \text{H}$  transition, but by  $N(\text{H}) \geq 3 \times 10^{22} \text{ cm}^{-3}$  (and  $n_{\text{H}}=10^{12} \text{ cm}^{-3}$ ), it becomes neutral. For higher densities though ( $n_{\text{H}}=10^{14} \text{ cm}^{-3}$ ) neutral atomic carbon dominates already from the BLR<sup>0</sup> surface. Regarding CO, for  $n_{\text{H}}=10^{12} \text{ cm}^{-3}$ , its abundance reaches  $X(\text{CO}) \sim 10^{-4}$  only when  $N(\text{H}) \geq 8 \times 10^{25} \text{ cm}^{-2}$  is reached, but this transition happens much "shallower" within the BLR<sup>0</sup> column,  $N(\text{H}) \sim 6 \times 10^{24} \text{ cm}^{-3}$ , for higher densities ( $n_{\text{H}}=10^{14} \text{ cm}^{-3}$ ).

It is expected from the ionization potentials of Ca and Ca<sup>+</sup> of IP=6.11 eV and 11.87 eV respectively that these two species should be abundant in BLR<sup>0</sup> (Ferland & Persson 1989). Figure 1 and C.1 show that the CaII abundance remains nearly constant across the entire BLR<sup>0</sup> for  $n_{\text{H}}=10^{12} \text{ cm}^{-3}$ , and only for the high-density model ( $n=10^{14} \text{ cm}^{-3}$ ), and large column densities ( $\geq 6 \times 10^{25} \text{ cm}^{-3}$ ), does its abundance drop sharply due to e<sup>-</sup> recombination into Ca, while Ca-bearing molecules have very low abundances in all models. Only depletion onto dust grains can change the gas-phase elemental abundance of Calcium, which is not an option in dustless BLRs.

Figure 2 shows the  $N(\text{H})$ -averaged abundances of H<sub>2</sub>, O, C, CO, OH, and H<sub>2</sub>O. The attenuation of the ionizing and molecule-dissociating radiation results into neutral and molecular species becoming abundant in BLR<sup>0</sup>. Nevertheless H<sub>2</sub> itself remains only a trace species except at the highest densities and largest column densities where  $X(\text{H}_2) \sim 0.1$  (Fig. 2, upper left). At high gas densities and temperatures up to  $\sim 1000 \text{ K}$ , e<sup>-</sup> recombination, neutral-neutral reactions with activation energy, and potentially three-body reactions are rapid because photoionization rates are  $\propto n_{\text{H}}$  while recombination rates are  $\propto n_{\text{H}}^2$ . These reactions can overcome the (neutral-atom/molecule)-destructive reactions such as photoionization, collisional ionization, photodissociation, and the collisional molecular dissociation. The OH abundance is higher than that of H<sub>2</sub>O in the  $n_{\text{H}} = 10^{12} \text{ cm}^{-3}$  model but remains as a secondary O-carrier, while for the highest density model ( $n_{\text{H}} = 10^{14} \text{ cm}^{-3}$ ) and at  $N(\text{H})$ , water is the second most abundant oxygen carrier.

The chemical molecule-formation path in dense and hot gas starts with H<sub>2</sub> formation in the presence of sufficient C<sup>+</sup>, C, and O. In the absence of dust grains, H<sub>2</sub> is then formed solely via gas-phase reactions (Crosas & Weisheit 1993). Once formed H<sub>2</sub> reacts with atomic oxygen to form OH, which in turn can react with H<sub>2</sub> to form H<sub>2</sub>O, or with singly-ionised carbon to form

<sup>3</sup> This is an important parameter in any radiative transfer model as it regulates the escape probability of spectral line emission, gas cooling, and thus gas thermodynamics.

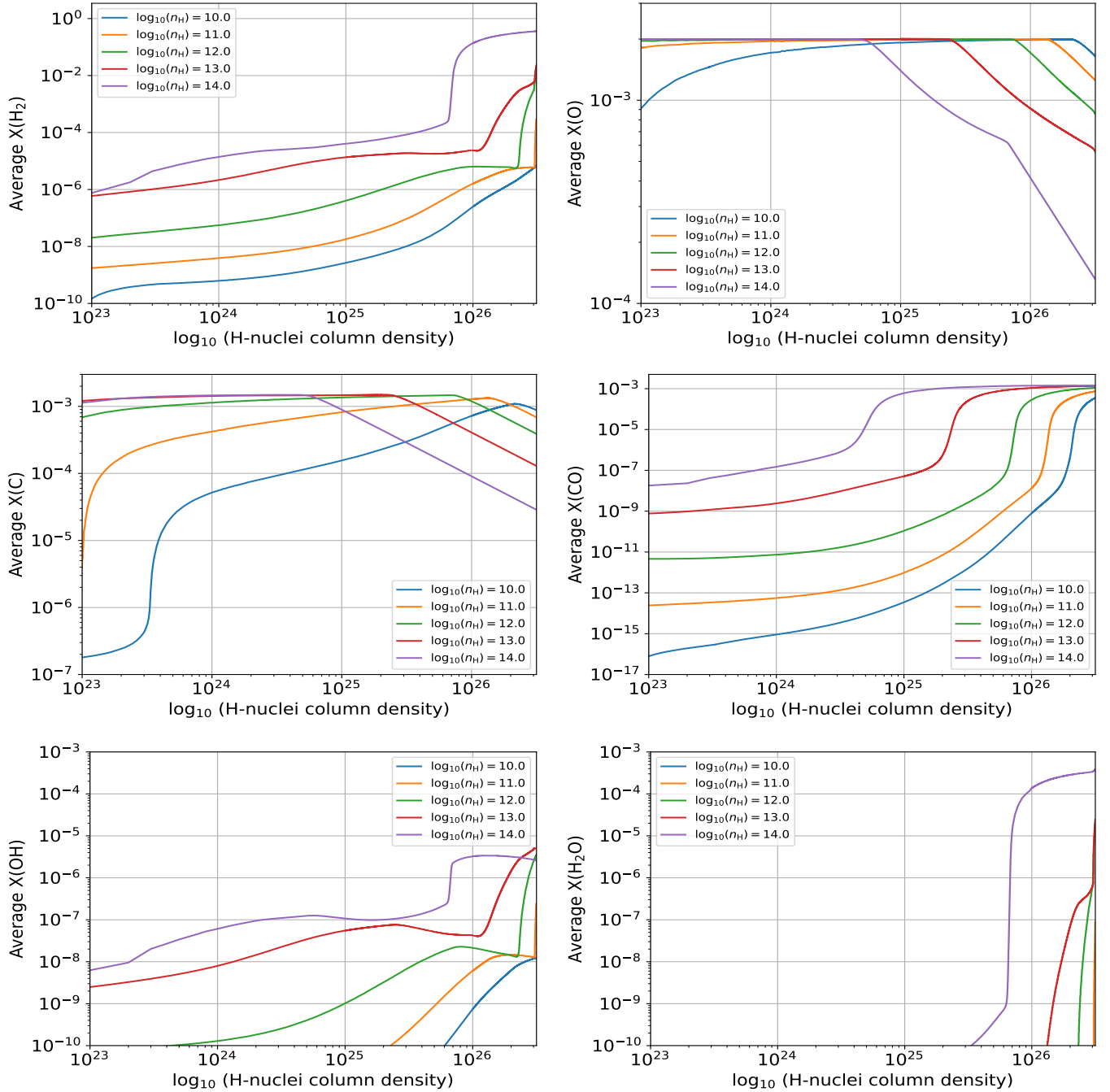


**Fig. 2.** Column density-averaged abundances for  $\text{H}_2$ , O, C, CO, OH, and  $\text{H}_2\text{O}$ . The total H-column density varies slightly between models as the grid is determined by the code.

CO via the reaction  $\text{C}^+ + \text{OH} \rightarrow \text{CO}^+$ , followed by  $\text{CO}^+ + \text{H} \rightarrow \text{CO} + \text{H}^+$  (Elitzur 1979; Hollenbach & McKee 1989; Thi & Bik 2005), see Appendix F. Alternatively, OH can react with C to form directly CO at very high densities. In the absence of dust grains, atomic C,  $\text{H}_2$  and CO molecules are shielded against photodissociation solely via line absorption, although the large intrinsic turbulence width decreases significantly the efficacy thereof. The CO/ $\text{H}_2$  ratio is much higher than in the ordinary dusty molecular ISM, making CO the most abundant molecule, and its lines potentially good BLR<sup>0</sup> tracers. Furthermore atomic oxygen, atomic carbon, OH,  $\text{H}_2\text{O}$ , and CO, once formed, they act as very efficient gas coolants, strongly impacting the gas thermal states, decreasing their temperature in deeper

BLR<sup>0</sup> layers. In principle this can push gas temperatures below the dust sublimation limit ( $\sim 1000\text{--}1500$  K, see Appendix E), allowing some dust to survive. Even trace amounts of dust surviving under BLR<sup>0</sup> conditions can have a very strong impact on  $\text{H}_2$  formation, and make the BLR<sup>0</sup> very  $\text{H}_2$ -rich (Crosas & Weisheit (1993)). When very few dust grains survive in BLR<sup>0</sup>, the enhanced  $\text{H}_2$  formation is due to the dust-enhanced attenuation of the molecule-dissociating AGN radiation field rather than to the classical  $\text{H}_2$  formation route on dust grains. Indeed even at  $T_{\text{dust}} \sim 600$  K, the grains are still too warm to allow efficient formation of  $\text{H}_2$  on their surfaces (Thi et al. 2020), while even little dust can strongly attenuate the photodissociating far-UV flux, enhancing molecule formation. At the same time, gas-

grain collisions, along with molecules, will cool the gas rapidly especially at high gas densities, enhancing the conditions for more molecule formation. Finally  $\text{H}_2$  can also form on PAHs (Boschman et al. 2015), which can survive in the hot environments of BLRs where silicate dust grains cannot. Thus inclusion of dust grains and PAHs in BLRs can further enhance the abundance of the molecular species such as  $\text{H}_2$  and CO in their BLR<sup>0</sup>. Here we must also note that for the inwards increasing gas density profiles expected in Radiation Pressure Confined (RPC) BLR models (Baskin, Laor, & Stern (2014)), the neutral atomic and molecular species abundances within BLR<sup>0</sup>'s can only be higher than those found for our uniform-density models.

Finally for the strongly UV-deficient AGN SEDs associated with low  $(dM/dt)/M_{\text{SMBH}}^2$  ratios (i.e. low accretion rates and/or hypermassive Black Holes, Laor & Davis (2011)), their BLRs are expected to be even more (neutral atom)/molecule-rich, perhaps even completely lacking a BLR<sup>+</sup> as an outside layer of the BLR<sup>0</sup> (yielding the so-called true Type 1 AGN). These cases, along with the effects of small amounts of dust and PAHs and assuming a disk BLR configuration (as indicated by high resolution BLR observations GRAVITY Collaboration (2018)) will be the subject of a forthcoming paper.

#### 4.1. The BLR<sup>0</sup> lines: a new spectral window to AGN, and extreme gas velocity fields near SMBHs

Atomic Oxygen can emit a series of lines in the UV/optical/near-IR and far-IR wavelength regimes (Bhatia & Kastner (1995) their Table 2). From these only its two fine structure lines at  $63.17\text{ }\mu\text{m}$  and  $145.5\text{ }\mu\text{m}$  (due to  $\text{L}\cdot\text{S}/r^3$ -type interaction term) can emanate from the BLR<sup>0</sup>, where the prevailing conditions are adequate for their collisions excitation up to full LTE levels. The rest of the O<sub>1</sub> lines, by involving energy transitions between the ( $n$ ,  $J$ ) principal quantum numbers, are energetically too demanding to be collisionally excited within BLR<sup>0</sup>'s. Pumping by Ly $\beta$  photons is necessary for the near-IR O<sub>1</sub> lines to be excited, placing them in the so-called low-ionization regions of the BLR<sup>+</sup> (where such photons are readily available). Dias dos Santos et al. (2023) has recently detected a very wide, double peak, O<sub>1</sub> near-IR line ( $\lambda 11297$ ) in Zw 002 (Seyfert I), which may indeed be marking the low-ionization layer of a BLR<sup>+</sup>. The two fine structure lines of C<sub>1</sub> at  $\sim 492\text{ GHz}$  and  $\sim 809\text{ GHz}$ , along with the  $J$ -rotational lines of CO, with  $J=1-0$  (115 GHz) up to  $J=6-5, 7-6$  (691 GHz, 806 GHz) are accessible through the Earth's atmosphere, and will be LTE-excited in a BLR<sup>0</sup>. Deep ALMA observations, while they cannot resolve C<sub>1</sub> and CO line emission in a BLR<sup>0</sup>, they can identify broad BLR<sup>0</sup> lines provided that multi-tuned ALMA correlator setups are used to cover the  $\sim(\text{few})\times(10^3-10^4)\text{ km s}^{-1}$  velocity range. The highest- $J$  CO lines accessible through the atmosphere (i.e.  $J=6-5, 6-7$ ) are the best choices since for LTE-excitation:  $\int_V S_v^{(\text{line})} dv \propto (J+1)^3 v_{\circ}^3 T_{\text{kin}}^{-4}$  ( $v_{\circ} \sim 115\text{ GHz}$ ). High resolution ALMA observations of high- $J$  CO lines of nearby AGN do exist, e.g. Gallimore et al. (2016), but their limited velocity coverage ( $\sim 600\text{ km s}^{-1}$ ), precludes them from identifying any ultra-wide BLR<sup>0</sup> CO line emission. Warm CO-rich gas can emit ro-vibrational lines in the near- and mid-IR, which are accessible for spatially resolved observations with IR interferometers such as GRAVITY+ or MATISSE at ESO. GRAVITY has already been used in the past to identify dustless hot and dense CO-rich gas around 51 Oph. Although water can be abundant

<sup>4</sup> Slightly redshifted AGN can be used to place such lines into much better atmospheric windows, without much sacrifice in received flux.

in the densest models, water lines are difficult to detect from ground-based telescopes and require a favorable redshift.

#### 4.2. Spectral line illumination of SMBHs: new GR tests?

Depending on their actual luminosities, the various neutral-atomic and/or molecular lines from the BLR<sup>0</sup> gas disk can provide a novel, *spectral line rather than continuum*, background illumination of the SMBHs in galactic centers. This can enable new tests of Kerr versus non-Kerr Spacetimes around these ultra-relativistic objects, as recently proposed by Kostaros, Papadopoulos, & Pappas (2024).

### 5. Conclusions

Our work demonstrated the likely presence of neutral atoms and CO molecules in a potentially massive neutral gas BLR<sup>0</sup> phase underlying the thin ionized layers of BLR<sup>+</sup> in AGN. In the dustless but warm and dense BLR<sup>0</sup> gas, the prevailing molecule is CO, while  $\text{H}_2$  remains only a trace species. Fine structure lines of neutral atomic Oxygen and Carbon at far-IR and submm wavelengths can uniquely trace the BLR<sup>0</sup> gas mass, while CO with its rotational and ro-vibrational CO lines at mm/submm and near-IR lines are also expected to be bright, opening a new observational spectral window to BLRs in AGN, and the extreme velocity fields near SMBHs. Gas density gradients, minute amounts of surviving dust (especially the thermally-resistant PAHs), and UV-photon deficient AGN SEDs (the result of low-accretion and/or hypermassive BHs in galactic centers), are all expected to further boost the abundances of neutral atoms and molecules in BLR<sup>0</sup> and will be studied in detail in a forthcoming paper.

*Acknowledgements.* We would like to offer thanks to the referee, that helped us clarify some finer, yet important, points in the presented work. PPP would like to acknowledge the hospitality of his colleague Wing-Fai Thi, in his apartment in Munich, where these ideas were developed.

### References

- Baskin, A., Laor, A., & Stern, J. 2014, MNRAS, 438, 604
- Baskin, A. & Laor, A. 2018, MNRAS, 472(2), 1970
- Baldwin, A. J., Ferland, G.J., Korista, K.T., Hamann, F., & Dietrich, M. 2003, ApJ, 582, 590
- Bhatia, A. K., & Kastner, S. O. 1995, ApJS, 96, 325
- Boschman, L., Cazaux, S., Spaans, M., et al. 2015, A&A, 579, A72. doi:10.1051/0004-6361/201323165
- Cazaux, S. & Tielens A. G. G. M. 2002, ApJ, 57, L29
- Crosas, M. & Weisheit, J. C. 1993, MNRAS, 262, 359
- Dewangan, G. C., Tripathi, P., Papadakis, I. E., & Singh K. P. 2021, MNRAS, Dias dos Santos, D., Rodríguez-Ardila, A., Panda, S., et al. 2023, ApJ, 953, L3. doi:10.3847/2041-8213/ace974
- Elitzur, M. 1979, ApJ, 229, 560. doi:10.1086/156989
- Elitzur, M. & Ho L. C. 2009, ApJ, 701, L91
- Ferland, G., & Persson, S. E. 1989, ApJ, 347, 656
- Ferland, G.: The broad emission line regions of quasars: Current status and future prospects. In: Richards, G.T., Hall, P.B. (eds.) AGN Physics with the Sloan Digital Sky Survey, vol. 311, p. 161. ASP Conference Series, San Francisco (2004)
- Gallimore J., Elitzur M., Maiolino R., et al. 2016, ApJ, 829, L7
- Gaskell, C.M.: What broad emission lines tell us about how active galactic nuclei work. New Astronomy Reviews 53(7-10), 140–148 (2009)
- GRAVITY Collaboration: Sturm et al. 2018 Nature, 563, 657
- GRAVITY Collaboration: Koutoulaki, M. et al. 2021, A&A, 645, 50
- Gould, R. J., & Salpeter, E. E. 1963, ApJ, 138, 393
- Gunasekera, C. M., van Hoof, P. A. M., Chatzikos, M., et al. 2023, Research Notes of the American Astronomical Society, 7, 246. doi:10.3847/2515-5172/ad0e75
- Hollenbach, D. & McKee, C. F. 1989, ApJ, 342, 306. doi:10.1086/167595
- Hollenbach, D. J. & Tielens, A. G. G. M. 1999, Reviews of Modern Physics, 71, 173. doi:10.1103/RevModPhys.71.173

Kallman, T., Lepp, S., & Giovannoni, P. 1987, *ApJ*, 321, 907

Korista, K. T., & Goad, M. R. 2004, *ApJ*, 606, 749

Kostaros, K., Papadopoulos, P., & Pappas, P. 2024 *Phys. Rev. D* Vol. 110, No. 2, 024001 – Published 2 July 2024

Laor, A., & Davies, S. W. 2011, *MNRAS*, 417, 681

Latter, W. B. & Black, J. H. 1991, *ApJ*, 372, 161. doi:10.1086/169961

Lepp, S., McCray, R., Shull, M., Woods, D. T., & Kallman, T. 1985, *ApJ*, 288, 58

Lepp, S., Dalgarno, A. & McCray, R. 1990, *ApJ*, 358, 262

McElroy D., Walsh C., Markwick A. J., Cordiner M. A., Smith K., Millar T. J., 2013, *A&A*, 550, A36

Millar, T. J., Walsh, C., Van de Sande, M., et al. 2024, *A&A*, 682, A109. doi:10.1051/0004-6361/202346908

Netzer, H.: AGN Emission Lines. In: Bradford, R.D., Netzer, H., Woltjer, L. (eds.) *Active Galactic Nuclei*, pp. 57–160. Saas-Fee Advanced Course of the Swiss Society for Astrophysics and Astronomy, Santa Fe (1990)

Peterson, B.M.: The Broad-Line Region in Active Galactic Nuclei. In: D., A., Johnson, R., Lira, P. (eds.) *Physics of Active Galactic Nuclei at All Scales*, 2006, vol. 693, pp. 77–100

Rokaki, E., Boisson, S., & Collin-Soufrin, S. 1992, *A&A*, 253, 57

Röllig, M., Abel, N. P., Bell, T., et al. 2007, *A&A*, 467, 187. doi:10.1051/0004-6361:20065918

Seyfert, C. 1948, *ApJ*, 97, 28

Shaw, G., Ferland, G. J., & Chatzikos, M. 2022, *ApJ*, 934, 53. doi:10.3847/1538-4357/ac7789

Shaw, G., Ferland, G., & Chatzikos, M. 2023, *Research Notes of the American Astronomical Society*, 7, 153. doi:10.3847/2515-5172/ace9b5

Spyromilio, J., Meikle, W. P. S., Learner, R. C. M., & Allen, D. A. 1988, *Nature*, 334, 327

Tatulli, E., Malbet, F., Ménard, F., G. C., Testi, L., Natta, A., Kraus, S., Stee, P., & Robbe-Dubois, S. 2008, *A&A*, 489, 1151

Thomas, A. D., Groves, B. A., Sutherland, R. S., Dopita, M. A., Kewley, L. J. & Jin, C. 2016 *ApJ*, 833, 266

Thi, W.-F., Ménard, F., Meeus, G. et al. 2013, *A&A*, 557, A111

Thi, W.-F. & Bik, A. 2005, *A&A*, 438, 557. doi:10.1051/0004-6361:20042219

Thi, W.-F., van Dalen, B., Bik, A., & Waters, L. B. F. M. 2005, *A&A*, 430, L61

Thi, W. F., Hocuk, S., Kamp, I., et al. 2020, *A&A*, 634, A42. doi:10.1051/0004-6361/201731746

## Appendix A: Three-body reactions

At densities  $> 10^{10} \text{ cm}^{-3}$ , the rate of three-body reactions becomes competitive with two-body reactions. Three-body formation and destruction reactions of  $\text{H}_2$  are accounted by default by the code. We complemented the reaction networks with three-body reactions taken from the UMIST2012 (McElroy et al. 2013).

**Table A.1.** Three-body (collider) reactions added to the standard CLOUDY network. The rate coefficients are taken from (McElroy et al. 2013). M designates H or  $\text{H}_2$ .

Reaction		
$\text{CO} + \text{H} + \text{M}$	$\rightarrow$	$\text{O} + \text{C} + \text{H} + \text{M}$
$\text{CO} + \text{H}_2 + \text{M}$	$\rightarrow$	$\text{O} + \text{C} + \text{H}_2 + \text{M}$
$\text{CO} + \text{H} + \text{HOC}^+ + \text{M}$	$\rightarrow$	$\text{HCO}^+ + \text{CO} + \text{H} + \text{M}$
$\text{CO} + \text{H}_2 + \text{HOC}^+ + \text{M}$	$\rightarrow$	$\text{HCO}^+ + \text{CO} + \text{H}_2 + \text{M}$
$\text{C} + \text{O} + \text{H} + \text{M}$	$\rightarrow$	$\text{CO} + \text{H} + \text{M}$
$\text{C} + \text{O} + \text{H}_2 + \text{M}$	$\rightarrow$	$\text{CO} + \text{H}_2 + \text{M}$
$\text{H} + \text{O} + \text{H} + \text{M}$	$\rightarrow$	$\text{OH} + \text{H} + \text{M}$
$\text{H} + \text{O} + \text{H}_2 + \text{M}$	$\rightarrow$	$\text{OH} + \text{H}_2 + \text{M}$
$\text{H} + \text{OH} + \text{H} + \text{M}$	$\rightarrow$	$\text{H}_2\text{O} + \text{H} + \text{M}$
$\text{H} + \text{OH} + \text{H}_2 + \text{M}$	$\rightarrow$	$\text{H}_2\text{O} + \text{H}_2 + \text{M}$
$\text{H} + \text{CH}_3 + \text{H} + \text{M}$	$\rightarrow$	$\text{CH}_4 + \text{H} + \text{M}$
$\text{H} + \text{CH}_3 + \text{H}_2 + \text{M}$	$\rightarrow$	$\text{CH}_4 + \text{H}_2 + \text{M}$
$\text{H} + \text{NH}_2 + \text{H} + \text{M}$	$\rightarrow$	$\text{NH}_3 + \text{H} + \text{M}$
$\text{H} + \text{NH}_2 + \text{H}_2 + \text{M}$	$\rightarrow$	$\text{NH}_3 + \text{H}_2 + \text{M}$
$\text{H}_2 + \text{N} + \text{H} + \text{M}$	$\rightarrow$	$\text{NH}_2 + \text{H} + \text{M}$
$\text{H}_2 + \text{N} + \text{H}_2 + \text{M}$	$\rightarrow$	$\text{NH}_2 + \text{H}_2 + \text{M}$
$\text{O} + \text{O} + \text{H} + \text{M}$	$\rightarrow$	$\text{O}_2 + \text{H} + \text{M}$
$\text{O} + \text{O} + \text{H}_2 + \text{M}$	$\rightarrow$	$\text{O}_2 + \text{H}_2 + \text{M}$
$\text{H}_2 + \text{C} + \text{H} + \text{M}$	$\rightarrow$	$\text{CH}_2 + \text{H} + \text{M}$
$\text{H}_2 + \text{C} + \text{H}_2 + \text{M}$	$\rightarrow$	$\text{CH}_2 + \text{H}_2 + \text{M}$
$\text{H}_2 + \text{CH} + \text{H} + \text{M}$	$\rightarrow$	$\text{CH}_3 + \text{H} + \text{M}$
$\text{H}_2 + \text{CH} + \text{H}_2 + \text{M}$	$\rightarrow$	$\text{CH}_3 + \text{H}_2 + \text{M}$
$\text{C} + \text{N} + \text{H} + \text{M}$	$\rightarrow$	$\text{CN} + \text{H} + \text{M}$
$\text{C} + \text{N} + \text{H}_2 + \text{M}$	$\rightarrow$	$\text{CN} + \text{H}_2 + \text{M}$
$\text{C}^+ + \text{O} + \text{H} + \text{M}$	$\rightarrow$	$\text{CO}^+ + \text{H} + \text{M}$
$\text{C}^+ + \text{O} + \text{H}_2 + \text{M}$	$\rightarrow$	$\text{CO}^+ + \text{H}_2 + \text{M}$
$\text{C} + \text{O}^+ + \text{H} + \text{M}$	$\rightarrow$	$\text{CO}^+ + \text{H} + \text{M}$
$\text{C} + \text{O}^+ + \text{H}_2 + \text{M}$	$\rightarrow$	$\text{CO}^+ + \text{H}_2 + \text{M}$

## Appendix B: Additional reaction

The reaction  $\text{H} + \text{CO}$  has two branches:  $\text{H} + \text{C} + \text{O}$  and  $\text{C} + \text{OH}$ . For completeness, we also added the reaction  $\text{H} + \text{CO} \rightarrow \text{C} + \text{OH}$ , which has an activation energy of 77700 K, to the CLOUDY network. In our models, the  $\text{H} + \text{C} + \text{O}$  outcome dominates over the formation of OH.

## Appendix C: Calcium chemistry

CLOUDY accounts by default for the ionization and recombination of atomic and ionized Ca. We complemented the default network with chemical reactions that includes Ca-bearing molecules. The reactions and rates are taken from the UMIST2022 network (Millar et al. 2024). The abundance for the Ca-bearing species for the two typical models are shown in Fig. C.1. The molecular Ca-species are at most two orders of magnitude less abundant than Ca or  $\text{Ca}^+$ . In the high density model ( $n_{\text{H}} = 10^{14} \text{ cm}^{-3}$ ), atomic Ca is the most abundance Ca-species so that the CaII lines probe only a fraction of the total neutral gas at high column densities.

**Table C.1.** Ca species reactions added to the standard CLOUDY network. The rate coefficients are taken from (Millar et al. 2024). Reactios with CRPHOT are Cosmic-Ray induced photoionization reactions and reactions with PHOTON are Far-UV photodissociation reactions.

Reaction		
$\text{Ca} + \text{CRPHOT}$	$\rightarrow$	$\text{Ca}^+ + \text{e}^-$
$\text{CaO} + \text{CRPHOT}$	$\rightarrow$	$\text{Ca} + \text{O}$
$\text{CaOH} + \text{CRPHOT}$	$\rightarrow$	$\text{Ca} + \text{OH}$
$\text{Ca} + \text{OH}$	$\rightarrow$	$\text{CaO} + \text{H}$
$\text{Ca} + \text{H}_2\text{O}$	$\rightarrow$	$\text{CaO} + \text{H}_2$
$\text{Ca} + \text{H}_2\text{O}$	$\rightarrow$	$\text{CaOH} + \text{H}$
$\text{Ca} + \text{CO}_2$	$\rightarrow$	$\text{CaO} + \text{CO}$
$\text{Ca} + \text{O}_2$	$\rightarrow$	$\text{CaO} + \text{O}$
$\text{CaO} + \text{H}$	$\rightarrow$	$\text{Ca} + \text{OH}$
$\text{CaO} + \text{H}_2$	$\rightarrow$	$\text{Ca} + \text{H}_2\text{O}$
$\text{CaO} + \text{O}$	$\rightarrow$	$\text{Ca} + \text{O}_2$
$\text{CaO} + \text{CO}$	$\rightarrow$	$\text{Ca} + \text{CO}_2$
$\text{CaOH} + \text{H}$	$\rightarrow$	$\text{Ca} + \text{H}_2\text{O}$
$\text{CaOH} + \text{H}$	$\rightarrow$	$\text{CaO} + \text{H}_2$
$\text{CaO} + \text{PHOTON}$	$\rightarrow$	$\text{Ca} + \text{O}$
$\text{CaOH} + \text{PHOTON}$	$\rightarrow$	$\text{Ca} + \text{OH}$

## Appendix D: Photodissociation and self-shielding

Self-shielding against photodissociation for  $\text{H}_2$  and CO are accounted for by the code as illustrated by Fig. D.1. In the figure, the photodissociation rates for  $\text{H}_2$  and CO drop suddenly as soon as the relevant threshold column density is reached.

## Appendix E: The BLR gas temperature profile

The gas temperature as function of depth for the  $10^{12}$  and  $10^{14} \text{ cm}^{-3}$  models are shown in Fig. E.1 and Fig. E.2. The gas temperatures decrease with depth as photons are absorbed and cooler and molecular gas are more efficient gas coolants.

## Appendix F: $\text{H}_2$ and CO main formation and destruction

Figure F.1 illustrates the main formation and destruction routes for  $\text{H}_2$  and CO at steady-state for a model with density of  $10^{12} \text{ cm}^{-3}$ . The main reaction that actually forms  $\text{H}_2$  from simpler H atoms is  $\text{H}_2$  radiative recombination reaction.  $\text{H}_2$  is destroyed at high column density by the formation of OH, which can react with C to form CO. OH is formed by the reaction  $\text{O} + \text{H}_2$  with an activation barrier of  $\sim 4000 \text{ K}$ . This reaction is only relevant for gas hotter than  $\sim 1000 \text{ K}$ . The current network does not account for vibrational-excited  $\text{H}_2$  reactions. OH can react with H to reform  $\text{H}_2$ . At low column density CO is mostly destroyed by photodissociation. At column densities greater than  $10^{26} \text{ cm}^{-2}$  various reactions involving ions ( $\text{N}^+$ ,  $\text{OH}^+$ ,  $\text{He}^+$  contribute to the CO destruction. A detailed discussion of the reaction paths can be found in Thi & Bik (2005). The  $\text{H}_2$  formation via the radiative association  $\text{H} + \text{H}$  is very low and its rate depends on the excitation state of H (Latter & Black 1991). In our models, the radiative association reaction is only important at very low column densities.

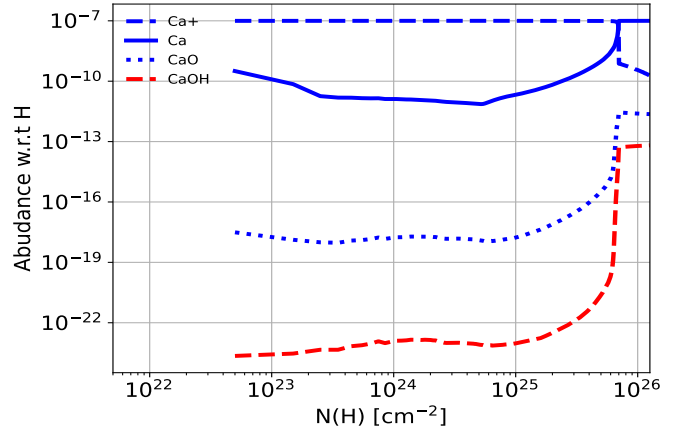
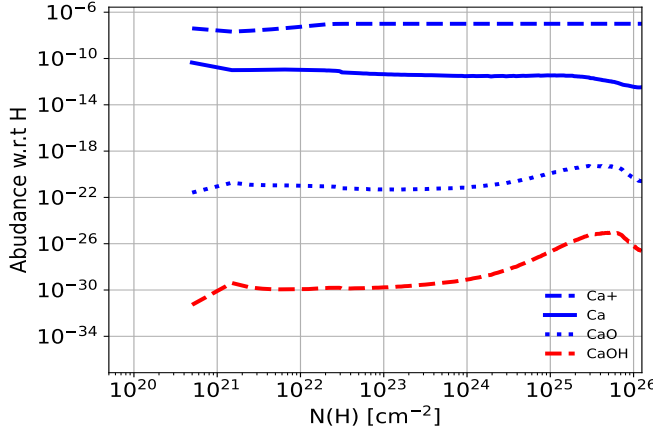


**Fig. C.1.** Abundance for Ca-bearing species as function of the column density, *Left*: A model with  $n_{\text{H}} = 10^{12} \text{ cm}^{-3}$ ,  $\log(U) = -3$ ,  $\Delta V = 250 \text{ km s}^{-1}$ , *Right*: A model with  $n_{\text{H}} = 10^{14} \text{ cm}^{-3}$ ,  $\log(U) = -5$ ,  $\Delta V = 250 \text{ km s}^{-1}$ .

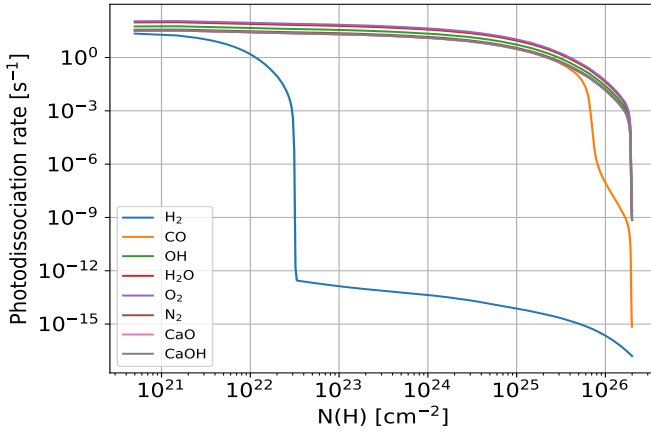


**Fig. D.1.** Gas temperature profile for a model with  $n_{\text{H}} = 10^{12} \text{ cm}^{-3}$ ,  $\log(U) = -3$ ,  $\Delta V = 250 \text{ km s}^{-1}$ .

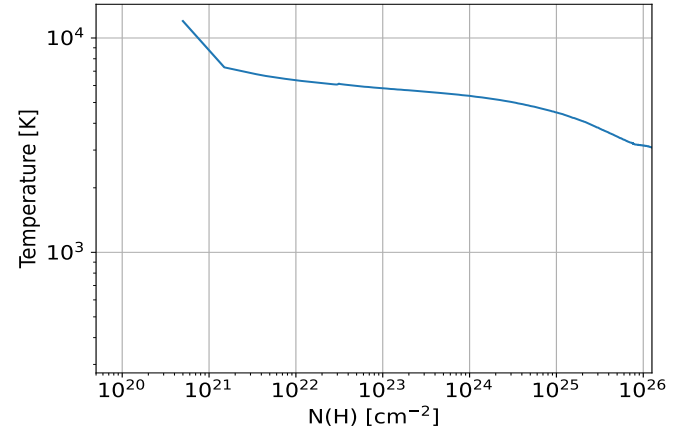


**Fig. E.1.** Gas temperature profile for a model with  $n_{\text{H}} = 10^{12} \text{ cm}^{-3}$ ,  $\log(U) = -3$ ,  $\Delta V = 250 \text{ km s}^{-1}$ .

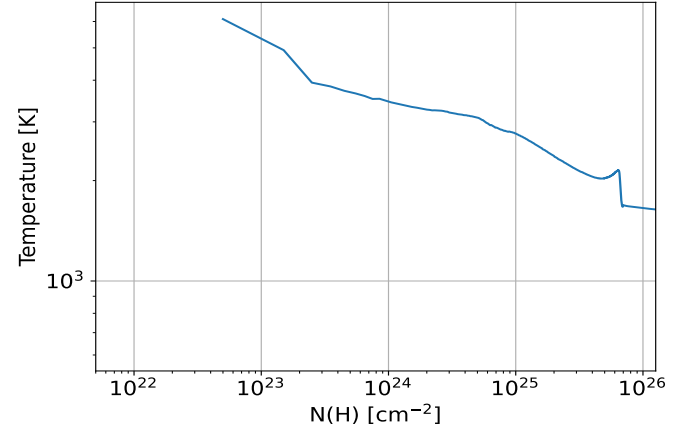


**Fig. E.2.** Gas temperature profile for a model with  $n_{\text{H}} = 10^{14} \text{ cm}^{-3}$ ,  $\log(U) = -5$ ,  $\Delta V = 250 \text{ km s}^{-1}$ .

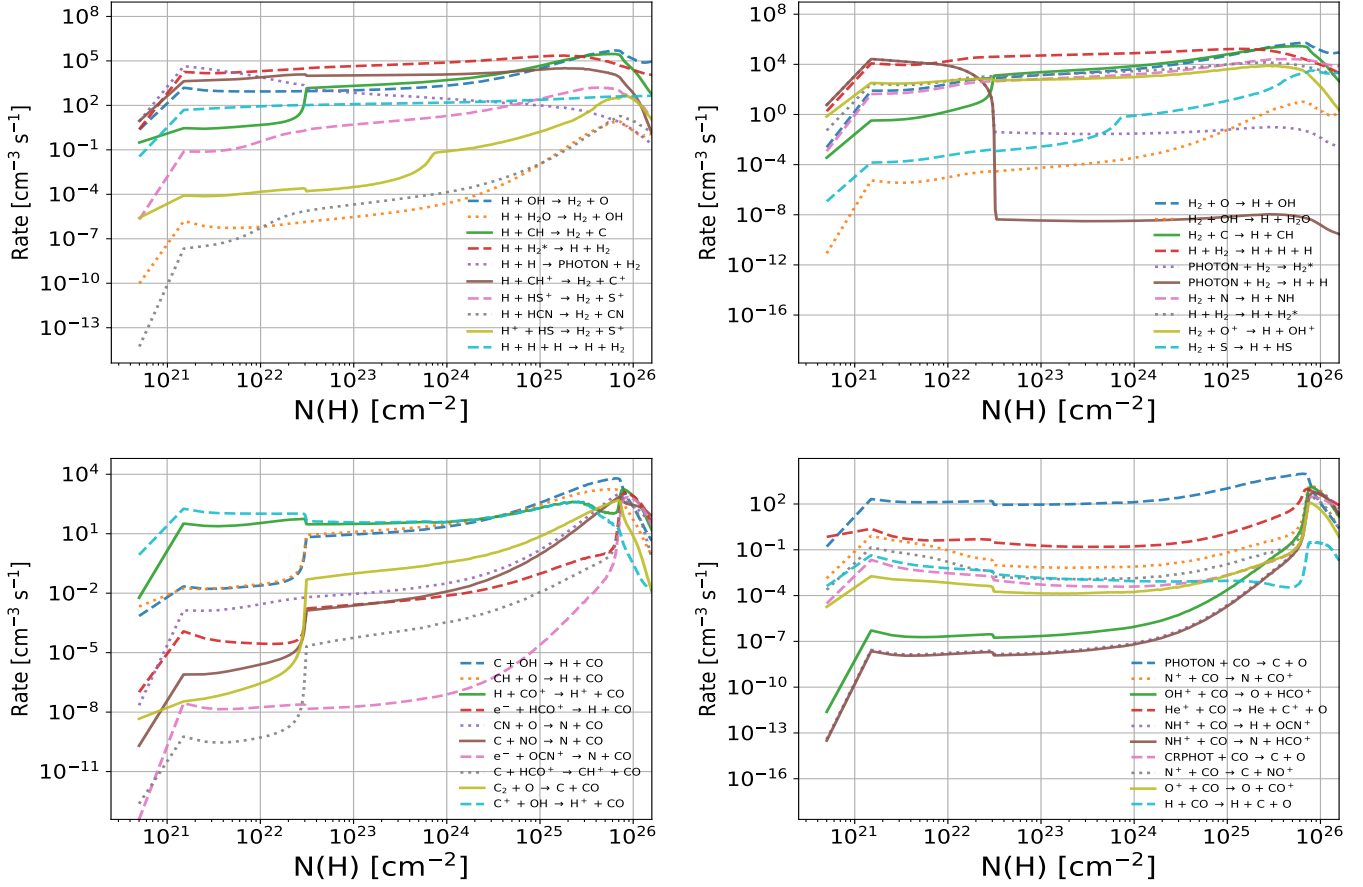


**Fig. F.1.** Main formation (left panels) and destruction (right panels) reactions for H $_2$  and CO for the  $n_H = 10^{12}$  cm $^{-3}$ ,  $\log(U) = -3$ ,  $\Delta V = 250$  km s $^{-1}$  model. Only the top 10 main formation and destruction reactions are shown